Biomaterials 84 (2016) 184–195

Contents lists available at ScienceDirect

Biomaterials

journal homepage: www.elsevier.com/locate/biomaterials

Planar and tubular patterning of micro and nano-topographies on poly(vinyl alcohol) hydrogel for improved endothelial cell responses

Marie F.A. Cutiongco [a, b, 1, 2], Seok Hong Goh [a, c, 1, 3], Rachida Aid-Launais [d, 4], Catherine Le Visage [d, e, 5], Hong Yee Low [c, f, **], Evelyn K.F. Yim [a, b, g, h, *]

[a] Department of Biomedical Engineering, National University of Singapore, Singapore
[b] Mechanobiology Institute, National University of Singapore, Singapore
[c] Institute of Materials Research and Engineering, Agency for Science, Technology and Research, Singapore
[d] INSERM, U1148, Laboratory for Vascular Translational Science, Paris, France
[e] INSERM, U791, Center for OstesArticular and Dental Tissue Engineering, Nantes, France
[f] Engineering Product Development Cluster, Singapore University of Technology and Design, Singapore
[g] Department of Surgery, National University of Singapore, Singapore
[h] Department of Chemical Engineering, University of Waterloo, 200 University Avenue West, Waterloo, Ontario, N2L 3G1, Canada

ARTICLE INFO

Article history:
Received 16 September 2015
Received in revised form
12 January 2016
Accepted 15 January 2016
Available online 20 January 2016

Keywords:
Endothelialisation
Surface modification
Surface topography
Vascular grafts
Three-dimensional
Luminal patterning

ABSTRACT

Poly(vinyl alcohol) hydrogel (PVA) is a widely used material for biomedical devices, yet there is a need to enhance its biological functionality for *in vitro* and *in vivo* vascular application. Significance of surface topography in modulating cellular behaviour is increasingly evident. However, hydrogel patterning remains challenging. Using a casting method, planar PVA were patterned with micro-sized features. To achieve higher patterning resolution, nanoimprint lithography with high pressure and temperature was used. *In vitro* experiment showed enhanced human endothelial cell (EC) density and adhesion on patterned PVA. Additional chemical modification via nitrogen gas plasma on patterned PVA further improved EC density and adhesion. Only EC monolayer grown on plasma modified PVA with 2 μm gratings and 1.8 μm concave lens exhibited expression of vascular endothelial cadherin, indicating EC functionality. Patterning of the luminal surface of tubular hydrogels is not widely explored. The study presents the first method for simultaneous tubular molding and luminal surface patterning of hydrogel. PVA graft with 2 μm gratings showed patency and endothelialization, while unpatterned grafts were occluded after 20 days in rat aorta. The reproducible, high yield and high-fidelity methods enable planar and tubular patterning of PVA and other hydrogels to be used for biomedical applications.

1. Introduction

Poly(vinyl alcohol) is a synthetic, non-toxic, non-immunogenic and biocompatible polymer for a number of biomedical applications [1,2]. Among the various methods of poly(vinyl alcohol) crosslinking studied, use of food-grade sodium trimetaphosphate (STMP) [3] in alkaline and ambient conditions creates poly(vinyl alcohol) hydrogel (heretofore referred to as PVA) with biocompatible, hemocompatible and mechanical properties appropriate for soft tissue engineering [4–7]. In addition, PVA can also be modified with plasma to change surface wetting property and chemistry without changing its bulk mechanical properties [8]. However, previous studies showed poor cell adhesion on PVA films *in vitro* [8] and absence of endothelialization on PVA vascular graft *in vivo* [5]. The hydrophilicity of PVA is postulated to deter protein adsorption and cell adhesion, thereby necessitating its modification

* Corresponding author. Department of Chemical Engineering, University of Waterloo, 200 University Avenue West, Waterloo, Ontario, N2L 3G1, Canada.
** Corresponding author. Engineering Product Development, Singapore University of Technology and Design, 8 Somapah Drive, 487372, Singapore.
E-mail addresses: hongyee_low@sutd.edu.sg (H.Y. Low), eyim@uwaterloo.ca (E.K.F. Yim).
[1] Both authors contributed equally to this work.
[2] Department of Biomedical Engineering, National University of Singapore, E4-04-08, 4 Engineering Drive 3, 117583, Singapore.
[3] Institute of Materials Research and Engineering, Agency for Science, Technology and Research, Innovis #08-03, 2 Fusionopolis Way, 138634, Singapore.
[4] INSERM, U1148, Laboratory for Vascular Translational Science, X. Bichat Hospital, Paris, 75018, France.
[5] INSERM, U791, Center for OsteoArticular and Dental Tissue Engineering, UFR d'Odontologie de Nantes, 1 Place A. Ricordeau, Nantes, 44042, France.

http://dx.doi.org/10.1016/j.biomaterials.2016.01.036
0142-9612/

to further develop its soft tissue applications [7,8].

Cell behaviors such as adhesion [9], proliferation [10,11], endocytosis [12] and differentiation [10,13] can also be altered *in vitro* by surface topography. The ability to direct desired cell behaviors can be further exploited in hydrogel-based biomedical devices for enhanced tissue regeneration *in vivo*. For instance, topography presented in vascular grafts is proposed to mimic the endothelial cell (EC) topographical niche and induce self-endothelialization that will lead to improved efficacy [14,15]. However, the high aqueous content in crosslinked hydrogel networks is fundamentally incompatible with traditional lithography techniques. Although there have been efforts to pattern hydrogel through photolithography, this approach often involves cytotoxic photoinitiators [16,17] and is limited to sub-micron feature size [18–21].

Casting is commonly adopted in biological research due to its simplicity, low cost and versatility [22] with the potential for non-planar patterning [23]. However, only micron-size patterns have been achieved on hydrogels of polyacrylamide [24,25] and poly(-vinyl alcohol) [26]; this can be attributed to the poor wetting properties between hydrogel and mold. On the other hand, thermal-based nanoimprint lithography (NIL) is a high-resolution and high-throughput technique used for planar patterning down to 6 nm [27]. Although NIL has been shown to pattern water-soluble poly(vinyl alcohol) templates [28,29], patterning of poly(vinyl alcohol) hydrogel that is insoluble in aqueous environment has not been explored. Hence, casting and NIL techniques provide complementary techniques to pattern insoluble PVA with topography.

In this study, we hypothesized that topography can enhance endothelial cell responses on PVA. The study addresses the challenges in hydrogel patterning by presenting reproducible planar and tubular hydrogel patterning via casting and NIL patterning techniques. Overall, the study highlights the importance and the need for surface topography to push forward the use of patterned hydrogel for research and translational applications such as vascular and nerve tissue engineering.

2. Methods and materials

2.1. Preparation of crosslinking PVA solution

An aqueous solution of 10% (w/v) poly(vinyl alcohol) (SigmaAldrich, 85–124 kDa, 87–89% hydrolyzed) was crosslinked with 15% (w/v) sodium trimetaphosphate (SigmaAldrich) and 30% (w/v) NaOH [7]. The crosslinking PVA solution was centrifuged to remove bubbles and afterwards immediately used for casting (section 2.2) or NIL (section 2.3).

2.2. Planar patterning of PVA via casting method

Polydimethylsiloxane (PDMS; Sylgard 184, Dow Corning) molds with various geometries and dimensions were used for casting (Table 1). Patterned PDMS molds were fabricated by curing on silicon templates (NIL Technology, Denmark; and, NTT Advanced Technology, Japan). All PDMS molds were plasma treated with 8 cc/min oxygen gas and 85 W for 1 min. Crosslinking PVA solution was poured on top of the freshly plasma-treated PDMS mold, and centrifuged at 140 × *g* for 1 h before crosslinking at 18 °C and 75–80% humidity. Planar PVA patterned through casting method (casted PVA) were immersed in phosphate buffered saline (PBS) for demolding (Fig. 1A). PDMS casted on plain tissue-culture polystyrene was used as a mold for casting of unpatterned PVA.

2.3. Planar patterning of PVA via NIL method

Crosslinking PVA solution was spin-coated at 800 rpm for 40 s on a clean glass coverslip and dried at ambient condition for approximately 30 min until an opaque film was formed. The predried crosslinking PVA were imprinted using patterned PDMS molds at the temperature of 180 °C and pressure of 40 bar for 10 min using the NIL system (Obducat). Planar PVA patterned using NIL method (NIL PVA) was demolded in dry state and rinsed with PBS (Fig. 1B). PDMS casted on unpatterned polystyrene petri dish was used as a mold for unpatterned NIL PVA.

2.4. N_2 plasma modification of casted PVA

Casted PVA without and with selected topographies were dried overnight at ambient temperature and subsequently plasma modified with 10 cc/min N_2 gas at 50 W for 1 min (RIE plasma SIRIUS, Trion). Immediately after plasma modification, N_2 plasma modified PVA were used for water contact angle measurement (Section 2.8) and cell culture (Section 2.9).

2.5. Scanning electron microscopy of PVA

Planar PVA made by casting (n = 3) and NIL (n = 3) methods were air-dried overnight at ambient temperature then coated with 10 nm thick platinum (JEOL-JFC 1600 auto-fine coater). Freeze fracture using liquid nitrogen was performed on dried PVA samples for analysis of the cross sectional height of topographies. Patterns on PVA were visualized using scanning electron microscope (SEM; JEOL-JSM 6010LV and JEOL-JSM-7600) at high vacuum and accelerating voltage of 5–10 keV. SEM images were used to analyse the dimensions of topographies (ImageJ 1.46j), where at least 5 measurements were obtained for each sample. Hydrated planar PVA were observed through environmental SEM (ESEM; Philips XL 30 ESEM-FEG at 15 keV and 3.5 Torr) without prior sample preparation.

2.6. Atomic force microscopy of nanometer-sized topography

Tapping mode atomic force microscopy (AFM; Bruker Fast Scan AFM) at a speed of 1 Hz was used to determine height of 250 nm gratings on PDMS and NIL PVA. Analysis of data was performed using Gwyddion software (Czech Metrology Institute).

2.7. X-ray photoelectron spectroscopy of planar PVA

X-ray photoelectron spectroscopy (XPS; Kratos Analytical, UK) was used to study surface elemental composition for unpatterned PVA made from both casting and NIL methods. A standard monochromated aluminum X-ray source (1486.7 eV, 75 W) at 90° with respect to the PVA surface was used to capture survey and high-resolution spectra. Survey and high-resolution spectra were analyzed using CasaXPS (Kratos Analytical). Peak assignment on high-resolution C1s spectrum was performed as previously described [8,30,31]. Binding energy was reported in electron volts (eV).

2.8. Static water contact angle of planar PVA

Casted PVA without N_2 plasma treatment and NIL PVA were dried overnight at ambient temperature before static water contact angle was measured. Static water contact angle on N_2 plasma modified PVA were immediately measured within 2 h after plasma treatment. Distilled, deionized water (1 μl) was deposited on the surface of the planar PVA and contact angle was measured with VCA AutoFAST (AST Products, Inc). Contact angles on casted and NIL PVA with gratings were measured perpendicular to the gratings axis, as described previously [32].

Table 1
Dimensions of topography on planar patterned PVA using casting and nanoimprint lithography (NIL) method. Multiple measurements were made on scanning electron microscopy (SEM) images (n = 3). Measurement of height of nanometer sized gratings on PDMS and PVA were made using atomic force microscopy (AFM). Width measurements apply to gratings while diameter measurements apply to pillars and lens.* denotes a statistically significant difference in dimensions between PDMS mold and casted PVA,‡ denotes a statistically significant difference in dimensions between PDMS mold and NIL PVA, ^ denotes statistically significant difference in dimensions between casted and NIL PVA. No statistical differences were observed in dimensions of casted PVA with and without N_2 plasma treatment. NA denotes not applicable and indicates no samples made. ND denotes not determined and indicates no measurements made.

	Gratings			Pillars		Convex lens			Concave lens
	250 nm	10 μm	2 μm	10 μm	2 μm	10 μm	2 μm	1.8 μm	1.8 μm
PDMS mold									
Width or diameter (μm)	0.24 ± 0.04	10.2 ± 0.62*	1.96 ± 0.06*	10.3 ± 0.21*	1.45 ± 0.05‡	10.5 ± 0.23*	1.83 ± 0.05*	1.63 ± 0.06*	1.35 ± 0.12
Pitch (μm)	0.54 ± 0.05	19.1 ± 0.39*	3.87 ± 0.06‡*	19.2 ± 0.31*	4.04 ± 0.03*	19.7 ± 0.21*	3.88 ± 0.08*	2.03 ± 0.07	1.98 ± 0.08
Height (μm)	0.22 ± 0.01‡	6.74 ± 0.41	2.11 ± 0.76	8.37 ± 0.51	1.80 ± 0.15	ND	ND	ND	ND
Casted PVA									
Width or diameter (μm)	NA	7.65 ± 0.03*	1.35 ± 0.09*^	6.35 ± 0.31*	1.6 ± 0.39	7.56 ± 0.30*	1.42 ± 0.11*	1.28 ± 0.09*	1.28 ± 0.12
Pitch (μm)	NA	14.1 ± 0.26*	2.86 ± 0.24*^	17.5 ± 0.42*	3.33 ± 0.26*	15.1 ± 0.32*	2.82 ± 0.09*	1.76 ± 0.23	1.81 ± 0.20
Height (μm)	NA	3.41 ± 0.46*	1.48 ± 0.38	5.52 ± 0.57*	1.32 ± 0.53	ND	ND	ND	ND
NIL PVA									
Width or diameter (μm)	0.23 ± 0.02	NA	1.92 ± 0.21^	NA	1.94 ± 0.13‡	NA	NA	1.63 ± 0.06	NA
Pitch (μm)	0.51 ± 0.03	NA	4.44 ± 0.23‡^	NA	4.13 ± 0.32	NA	NA	2.03 ± 0.07	NA
Height (μm)	0.08 ± 0.02‡	NA	1.57 ± 0.23	NA	1.84 ± 0.20	NA	NA	ND	NA
Casted PVA with N_2 plasma modification									
Width or diameter (μm)	NA	NA	1.37 ± 0.09	NA	1.60 ± 0.25	NA	NA	1.34 ± 0.16	1.16 ± 0.24
Pitch (μm)	NA	NA	3.28 ± 0.62	NA	3.58 ± 0.40	NA	NA	2.02 ± 0.11	1.71 ± 0.15
Height (μm)	NA	NA	1.30 ± 0.14	NA	1.26 ± 0.23	NA	NA	ND	ND

2.9. Cell culture on planar PVA

Casted PVA (n = 4) and NIL PVA (n = 4) were placed in a 24-well plate and held down by Silastic tubing (Dow Corning). The corresponding unpatterned PVA fabricated using the same method as the tested patterned PVA were used as the controls. Casted and NIL PVA were rinsed with PBS, sterilized with UV light and immersed in 10% penicillin-streptomycin (PAA) and 1% amphotericin-B solution (Sigma Aldrich). Casted and NIL PVA were extensively washed in PBS. N_2 plasma modified PVA (n = 4) were only sterilized with UV light for 20 min. All PVA were incubated overnight at 4 °C with fetal bovine serum (FBS, Gibco) before human umbilical vein EC line EA.hy926 (ATCC) were seeded at a total of 50000 cells/cm^2 per film in complete culture medium according to the supplier's recommendation. Glass coverslip was included as a positive control.

Cell morphology and cell adhesion were assessed 24 h after cell seeding. Total cell number on planar PVA was quantified using CyQuant assay (LifeTechnologies). For cells morphology study, cells were fixed using 4% paraformaldehyde in PBS at 4 °C and stained with 4′,6-Diamidino-2-Phenylindole Dihydrochloride (DAPI, LifeTechnologies) and Alexa Fluor 488-labeled phalloidin (LifeTechnologies, 1:300 dilution) at room temperature. Images of cell cytoskeleton and nuclei were taken using epifluorescence microscope (Leica DmiRB) for further morphometric analysis (section 2.9).

Endothelial monolayer formation was then characterized on N_2 plasma modified PVA by culturing EA.hy926 cells for 6 days with complete medium replacement every 2 days. Afterwards, PVA were fixed with 4% paraformaldehyde and stained using anti-Vascular Endothelial-Cadherin (VE-cadherin; Cell Signaling Technology; 1:200 dilution) and anti-rabbit IgG Alexa Fluor-488 secondary antibody (Life Technologies, 1:500 dilution). Actin cytoskeleton and nuclei were stained as described above. Images of VE-cadherin, actin cytoskeleton and nuclei were taken using epifluorescence microscope (Leica DMiRB).

2.10. Cell morphometric analysis

Using images of cell cytoskeleton, individual cell boundaries were hand-drawn using the free-hand polygon selection tool on ImageJ (1.49v, National Institutes of Health). Cell area and circularity measurements were performed on at least 30 cells from each sample type (n = 2). Quantification of VE-cadherin fluorescence intensity at EC boundary was performed as previously described [11].

2.11. Tubular PVA patterning and characterization

Tubular patterning was performed to obtain topographies on the luminal surface of PVA (Fig. 1C). A patterned cylindrical mold was assembled by attaching a thin-film of patterned PDMS on rods with outer diameter of 2 mm. The assembled cylindrical mold was plasma-treated for 1 min at 85 W and 8 cc/min oxygen gas. Immediately after plasma treatment, assembled cylindrical molds were immersed in crosslinking PVA solution (section 2.1) followed by sonication at 53 kHz without heating (Kudos ultrasonic cleaner) for 1 h. After sonication, the cylindrical mold was repeatedly dip-casted in freshly-made crosslinking PVA solution. Tubular PVA were dried at 18 °C and 75–80% humidity. SEM characterization was done on the luminal surface of the tubular PVA as described in section 2.5. Mechanical properties of tubular patterned PVA grafts were studied as previously described [33]. Briefly, uniaxial tensile strength and suture retention were measured using INSTRON 3345. Burst pressure and radial compliance were measured on close-ended grafts. Digital images of graft cross sections taken with optical microscope (Nikon) were used to measure internal diameter and wall thickness.

2.12. In vivo implantation of tubular patterned PVA

Animal study was done in accordance with Principles of Laboratory Animal Care and with approval of the Animal Care and Use Committee of the Claude Bernard Institute (Paris, France). Adult male Wistar rats (450–600 g) were administered with sodium pentobarbital intraperitoneally (50 mg/kg). Under an operating stereomicroscope, the infrarenal aorta was exposed and ligated. A 1 cm segment of the infrarenal aorta was resected and replaced with PVA grafts with 2 μm gratings (n = 2), 2 μm pillars (n = 1), 1.8 μm convex lens (n = 1), 1.8 μm concave lens (n = 1) or without pattern (n = 1), using end-to-end anastomosis with Prolene sutures (10/0). No anticoagulants or antiplatelets were administered post-surgery. Upon explant, grafts were cryosectioned for standard

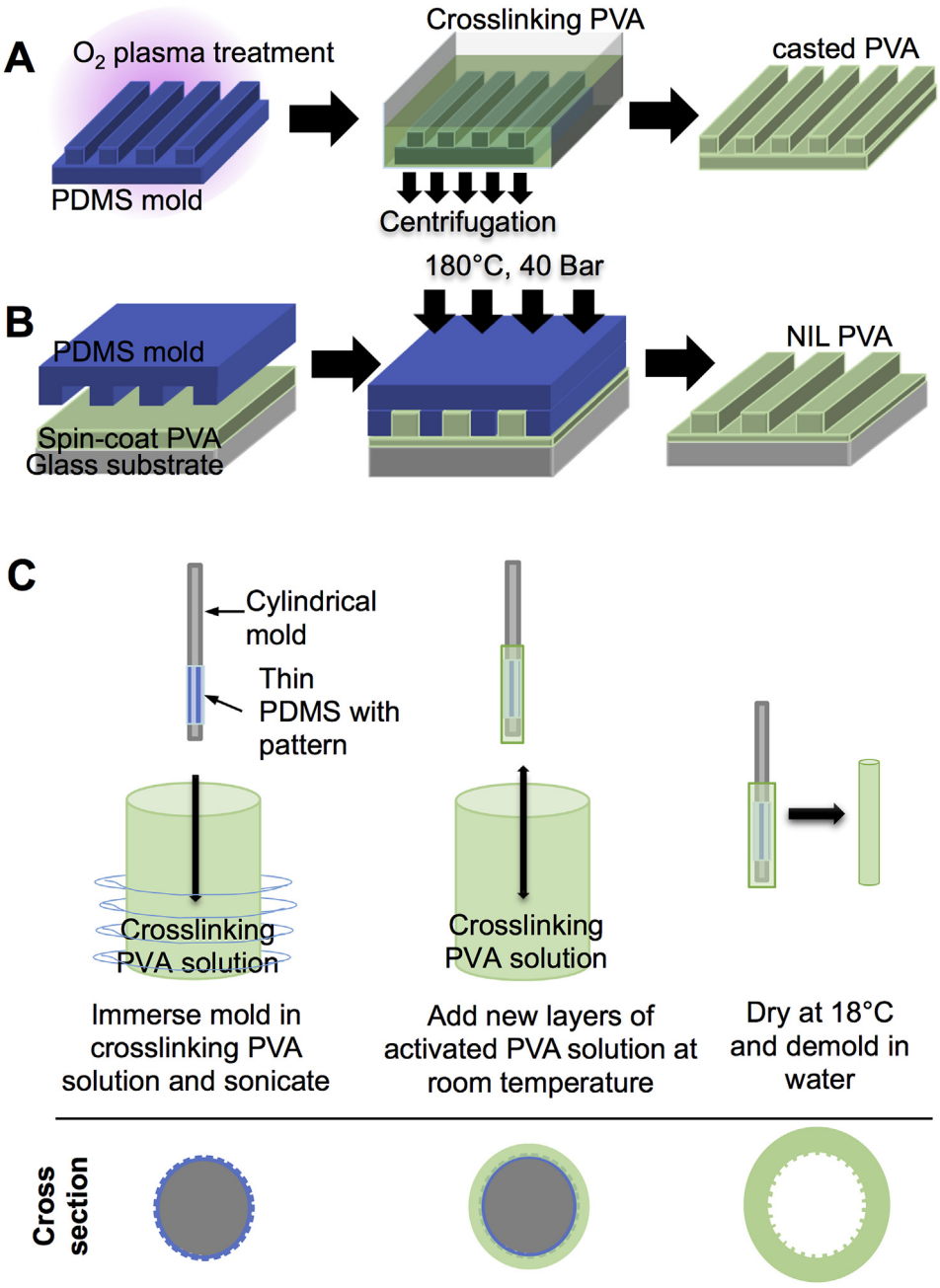

Fig. 1. Schematic diagram of patterning of poly(vinyl alcohol) (PVA). Patterning of planar PVA using (A) casting and (B) thermal-based nanoimprint lithography (NIL) methods. Unpatterned PVA films were made with either method and was used as an appropriate control to PVA films fabricated using the same method. (C) Dip-casting method for luminal patterning of PVA vascular graft. Blue denotes polydimethylsiloxane (PDMS) mold, green denotes PVA. (For interpretation of the references to colour in this figure legend, the reader is referred to the web version of this article.)

H&E and immunofluorescence staining against nucleus (DAPI) and RECA-1 antigen (AbD Serotec MCA970, 1:100). Low magnification hematoxylin and eosin (H&E) images were used to measure total luminal area and total patent area of each patent PVA graft. Patent luminal area was reported as total patent area normalized to total luminal area of each PVA graft.

2.13. Statistical analysis

Student's t-test was used to compare dimensions of topography between patterned planar PVA and PDMS mold, and mechanical properties between unpatterned and patterned tubular PVA. One-way ANOVA with Dunnett's post-hoc test was performed to compare water contact angle, cell density, cell area and VE-cadherin expression. Two-way ANOVA with Sidak's post-hoc test was used to compare water contact angle and cell morphology between unmodified and N_2 plasma modified PVA. Statistical significance was considered at $p < 0.05$. All data are presented as mean ± standard deviation.

3. Results

3.1. Patterning of planar PVA using casting and NIL methods

Periodic arrays of topographies on PVA were achieved via casting on PDMS molds (Fig. 2). The additional process of oxygen

plasma treatment of the PDMS mold and centrifugation force enhanced the filling of aqueous PVA solution into various structures on PDMS mold, showing 100% patterning yield of PVA (Figure S1). Diffraction of the films verified that the total patterned area on the PVA (approximately 1 cm^2) equalled the mold area (Figure S1) and high magnification SEM images showed that all topographies on casted PVA were well replicated with good shape fidelity (Fig. 2A, Figure S2). In addition, ESEM images verified that the topographies on casted PVA were still present in hydrated state of PVA without shape distortion (Fig. 2B). Furthermore, the topography on casted PVA were still present after 1 year of storage in PBS, attesting to the permanence and stability of the patterned PVA using casting method (Fig. 2C).

However, the geometrical dimensions of PVA topographies were different from those on the PDMS mold (Table 1). The differences observed between casted PVA and PDMS molds were most marked for large topographies such as 10 μm gratings, 10 μm pillars and 10 μm convex lens. Measurements made using ESEM images also showed a consistent reduction in topography size on casted PVA compared with those on the PDMS molds (Table S1). Despite the discrepancy in dimensions, excellent fidelity in shape and high yield of patterning of micron-sized features were observed on casted PVA. In contrast, nano-size features such as 250 nm gratings replicated via casting showed shape distortion and poor yield (Figure S3). To improve nano-size replication, NIL was performed on PVA.

Successful patterning of micon-size topography and nano-size topography was achieved with NIL (Fig. 2D). The micro-sized topographies fabricated using NIL had comparable dimensions with the PDMS mold (Table 1). In addition, NIL also improved the replication of nano-sized topography on PVA. Patterning of 250 nm gratings on PVA was achieved with fidelity in both shape and dimensions of the topography, which was not feasible with the casting method. ESEM also showed the presence of the topography on NIL PVA hydrogel after hydration, thus indicating stability of the patterned NIL PVA (Fig. 2E).

XPS verified that unpatterned PVA samples made through casting (C1s: 68.8 ± 0.40%, O1s: 30.8 ± 0.42%) and NIL (C1s: 64.3 ± 0.46%, O1s: 32.5 ± 0.26%) shared similar surface elemental composition. High-resolution C1s spectrum analysis also showed minute differences between unpatterned casted and NIL PVA in the methyl, hydroxyl, carbonyl and carboxyl group distribution (Fig. 3A and B). The results indicated that there were no substantial differences between the surface chemical composition of casted and NIL PVA. This further implied that no substantial changes occurred with the increased pressure and temperature used in NIL method.

Water contact angle analysis showed differences in water contact angle between the patterned and unpatterned PVA (Fig. 3C). Water contact angle on casted PVA with 2 μm gratings showed significant increase compared with unpatterned casted PVA. Meanwhile, casted PVA with 2 μm pillars, and 2 μm convex lens had markedly decreased water contact angle. Similar trends were observed in water contact angle values for NIL PVA samples (Fig. 3D). NIL PVA with 250 nm gratings showed a significant two-fold increase in water contact angle when compared with unpatterned NIL PVA.

3.2. Modification of casted PVA with N_2 plasma treatment

While topography influenced EC adhesion on casted PVA (section 3.3), N_2 plasma treatment was applied to casted PVA with selected topographies to further investigate EC adhesion and morphology. Notably, there was no significant change in the shape or dimensions of topographies between casted and N_2 plasma modified PVA (Fig. 4A, Table 1). XPS analysis of unpatterned PVA with N_2 plasma modification showed the presence of nitrogen content on the surface (Fig. 4B; C1s: 63.1%, O1s: 31.2%, N1s: 0.36%). Notably, N_2 plasma modified PVA with 2 μm gratings, 1.8 μm convex and concave lens showed significant increase in water contact angle compared with N_2 plasma modified PVA without pattern. Meanwhile, N_2 plasma modified PVA with 2 μm pillars showed significantly decreased water contact angle compared with unpatterned PVA with N_2 plasma modification. Two-way ANOVA analysis showed a significant increase in water contact angle in casted PVA (Fig. 3C) after N_2 plasma modification (Fig. 4C). Nonetheless, similar trends in water contact angle between patterned and unpatterned PVA were present in both casted and N_2 plasma modified PVA.

3.3. EC adhesion on patterned casted and NIL PVA

Adhesion of human ECs was investigated on casted and NIL PVA without and with different topographies (Fig. 5). Unpatterned PVA (obtained from both casting and NIL methods) showed low cell attachment with rounded cell morphology (Fig. 5A and B). In

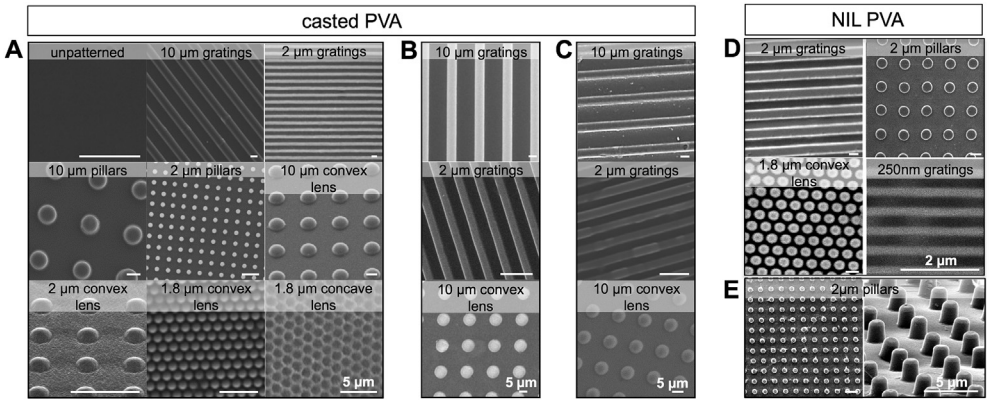

Fig. 2. Characterization of planar PVA with topography. Scanning electron microscopy (SEM) and environmental SEM (ESEM) images of PVA patterned films with various topography via casting (A, B, C) and NIL (D, E). (A) SEM showed successful patterning of topographies using casting method. Unpatterned casted PVA was also fabricated. Scale bar = 5 μm. (B) ESEM performed on selected casted PVA films showed the stability of patterning and the presence of topography in the hydrated state of the PVA hydrogel. Scale bar = 5 μm. (C) Casted PVA films stored in sterile phosphate buffered saline (PBS) for up to one year in ambient conditions retained its topography with shape and size similar to freshly patterned films. Scale bar = 5 μm. (D) SEM showed successful patterning of topographies using NIL method. Scale bar = 5 μm. (E) ESEM imaging on selected NIL PVA film showed stability of topography in the hydrated state of the NIL PVA in both low and high magnification. Scale bar = 2 μm.

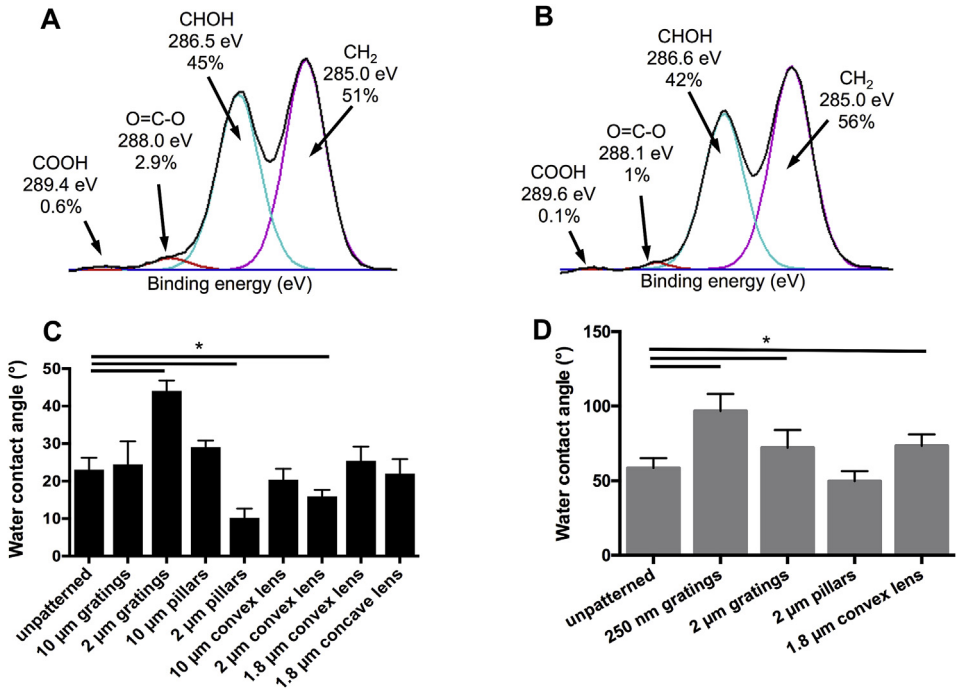

Fig. 3. Surface characterization of PVA films. X-ray photoelectron spectroscopy (XPS) characterization of unpatterned PVA films formed via (A) casting and (B) NIL. Binding energy is given in electron Volts (eV). (C) Static water contact angle measurement on casted PVA with different surface topography. (D) Static water contact angle measurement on NIL PVA with different surface topography. * denotes statistical significance using one-way ANOVA with $p < 0.001$.

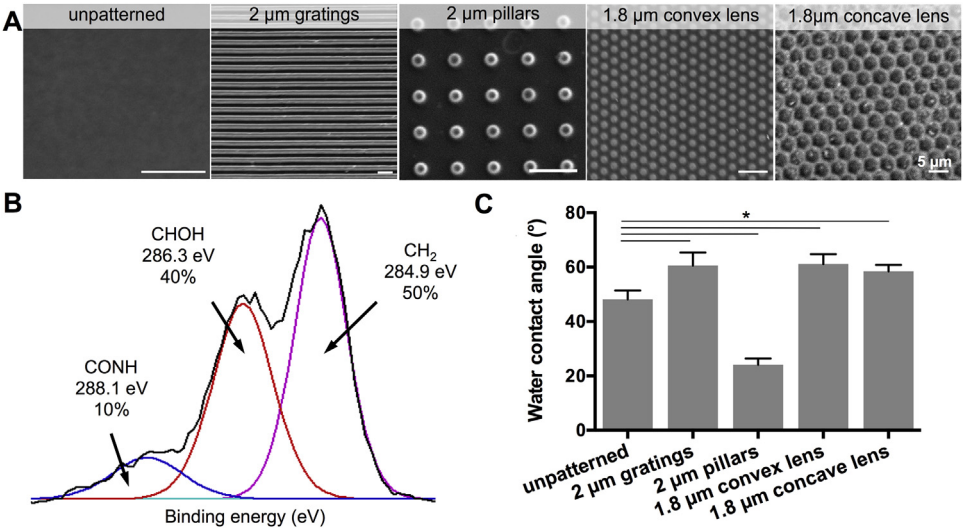

Fig. 4. Surface characterization of casted PVA film with topography and nitrogen gas (N_2) plasma modification. (A) SEM images of casted PVA films after N_2 plasma modification. N_2 plasma modification of casted PVA did not show distortion in shape of topography. Scale bar = 5 μm. (B) XPS showed presence of nitrogen on surface of casted PVA after N_2 plasma modification. Binding energy is given in eV. (C) Water contact angle analysis of casted PVA with N_2 plasma modification showed significant changes compared with N_2 plasma modified PVA without pattern. All casted PVA films with N_2 plasma modification showed significant increase in water contact angle when compared with the same patterned casted PVA films without N_2 plasma modification. * denotes statistical significance using one-way ANOVA with $p < 0.0001$.

general, casted PVA with topography showed increased cell attachment with more spread morphology after 24 h (Fig. 5A). ECs cultured on casted PVA with gratings exhibited some elongation while ECs grown on casted PVA with pillars and lens topographies retained a circular shape. Casted PVA with 10 μm gratings, 2 μm gratings, 1.8 μm convex and 1.8 μm concave lens promoted a significantly higher EC attachment as compared with unpatterned casted PVA (Fig. 5C). In contrast, casted PVA with 10 μm convex lens and 2 μm pillars negatively modulated cell adhesion. A similar trend of cell adhesion was observed on NIL PVA, where 2 μm gratings on PVA showed a more spread morphology (Fig. 5B) and a significant increase in cell attachment (Fig. 5D). While EC adhesion on NIL PVA with 250 nm gratings or 1.8 μm convex lens was unchanged from the unpatterned NIL PVA, the spread EC morphology on these films were notable. NIL PVA with 2 μm pillars also showed no change in EC adhesion compared to unpatterned NIL PVA, but EC morphology on these films were similar to casted PVA with 2 μm pillars.

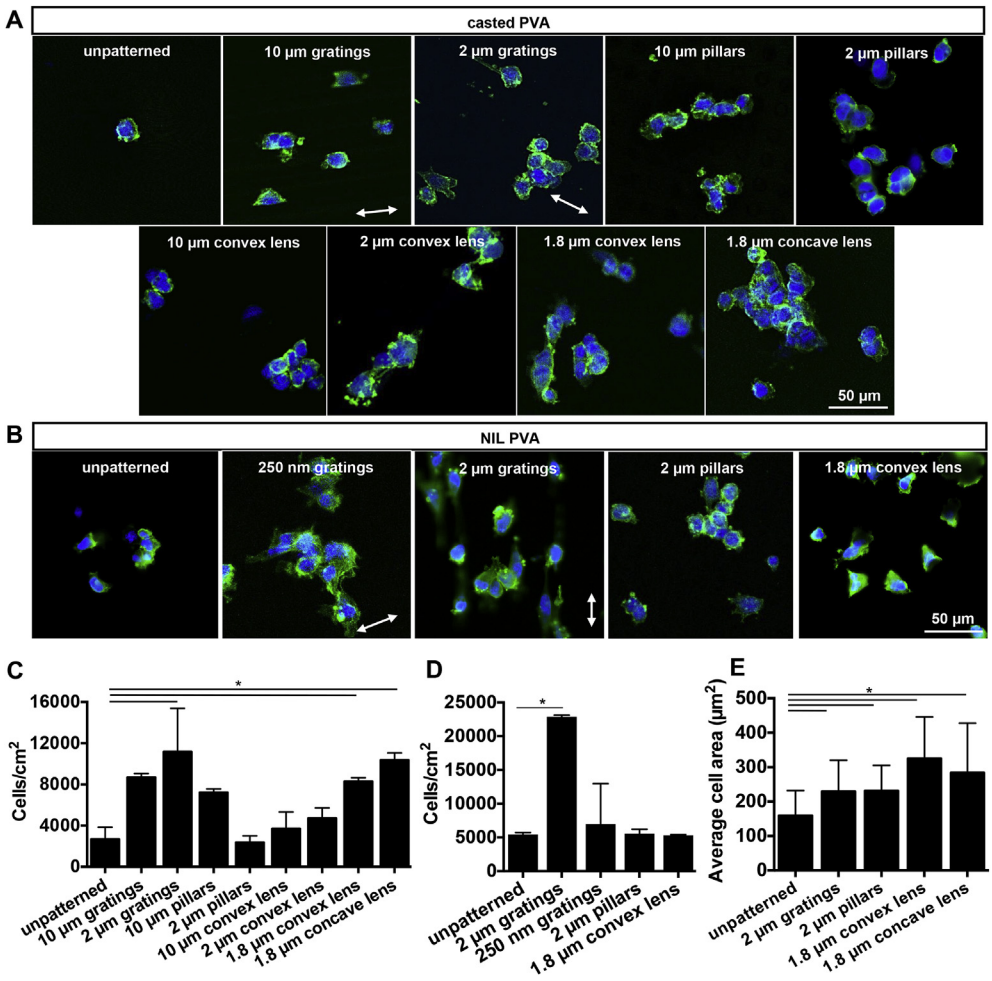

Fig. 5. Endothelial cell (EC) adhesion on planar PVA films patterned through casting and NIL methods. (A) Fluorescence images of cells on casted PVA films showed cell morphology. Unpatterned casted PVA was used as a control. Blue denotes nuclei while green denotes actin. White arrows denote gratings axis. Scale bar = 50 μm. (B) Fluorescence images of cells on NIL PVA films showed cell morphology. Unpatterned NIL PVA was included as control. Blue denotes nuclei while green denotes actin. White arrow denotes gratings axis. Scale bar = 50 μm. (C) Average cell density on casted PVA films with different topography. * denotes statistical significance using one-way ANOVA with $p < 0.05$. (D) Average cells density on NIL PVA films with different topography. * denotes statistical significance using one-way ANOVA with $p < 0.01$. (E) Analysis of EC area on selected casted PVA. * denotes statistical significance using one-way ANOVA. (For interpretation of the references to colour in this figure legend, the reader is referred to the web version of this article.)

Morphometric analysis of cell area and cell circularity was performed on casted PVA that significantly improved (2 μm gratings, 1.8 μm convex lens and 1.8 μm concave lens) or reduced (2 μm pillar) EC density. Cell area was significantly increased on casted PVA with topography as compared with unpatterned casted PVA (Fig. 5E). Notably, even EC grown on casted PVA with 2 μm pillars showed a significantly larger cell area in contrast to unpatterned casted PVA. Similarly, EC circularity was significantly changed on casted PVA (Figure S4A). EC grown on casted PVA with 2 μm gratings, 1.8 μm convex lens and 1.8 μm concave lens decreased in cell circularity compared with EC grown on unpatterned casted PVA. Meanwhile, cells grown on casted PVA with 2 μm pillars did not show any significant change in cell circularity.

3.4. EC adhesion on N_2 plasma modified PVA

Topographical modification improved EC adhesion on casted and NIL PVA but was insufficient to change the rounded morphology of cells to a more adherent shape. Thus, N_2 plasma modification was utilized to further improve EC adhesion and morphology on the selected casted PVA (2 μm gratings, 2 μm pillars, 1.8 μm concave lens, 1.8 μm convex lens and unpatterned). Modification of N_2 plasma modified PVA with topography improved EC adhesion (Fig. 6A). EC grown on N_2 plasma modified PVA with 2 μm gratings, 1.8 μm concave lens and unpatterned showed cells with spread morphology. In contrast, EC on N_2 plasma modified PVA with 2 μm pillars and 1.8 μm convex lens still retained the circular morphology that was observed on casted PVA (without plasma treatment). Overall EC density on N_2 plasma modified PVA significantly improved (with at least 10 times higher EC density, $p < 0.0001$) from casted PVA. Significant increase in EC adhesion was observed on N_2 plasma modified PVA with 2 μm gratings, 2 μm pillars and 1.8 μm concave lens when compared to the unpatterned PVA with N_2 plasma modification (Fig. 6B). In contrast, N_2 plasma modified PVA with 1.8 μm convex lens showed significant decrease in cell density when compared to unpatterned PVA with N_2 plasma modification.

VE-cadherin expression was detected in EC monolayer on N_2 plasma modified PVA with 2 μm gratings and 1.8 μm concave lens, similar to the expression when grown on glass coverslip (Fig. 6C). In contrast, EC monolayer on N_2 plasma modified PVA with 2 μm pillars, 1.8 μm convex lens or without pattern lacked VE-cadherin

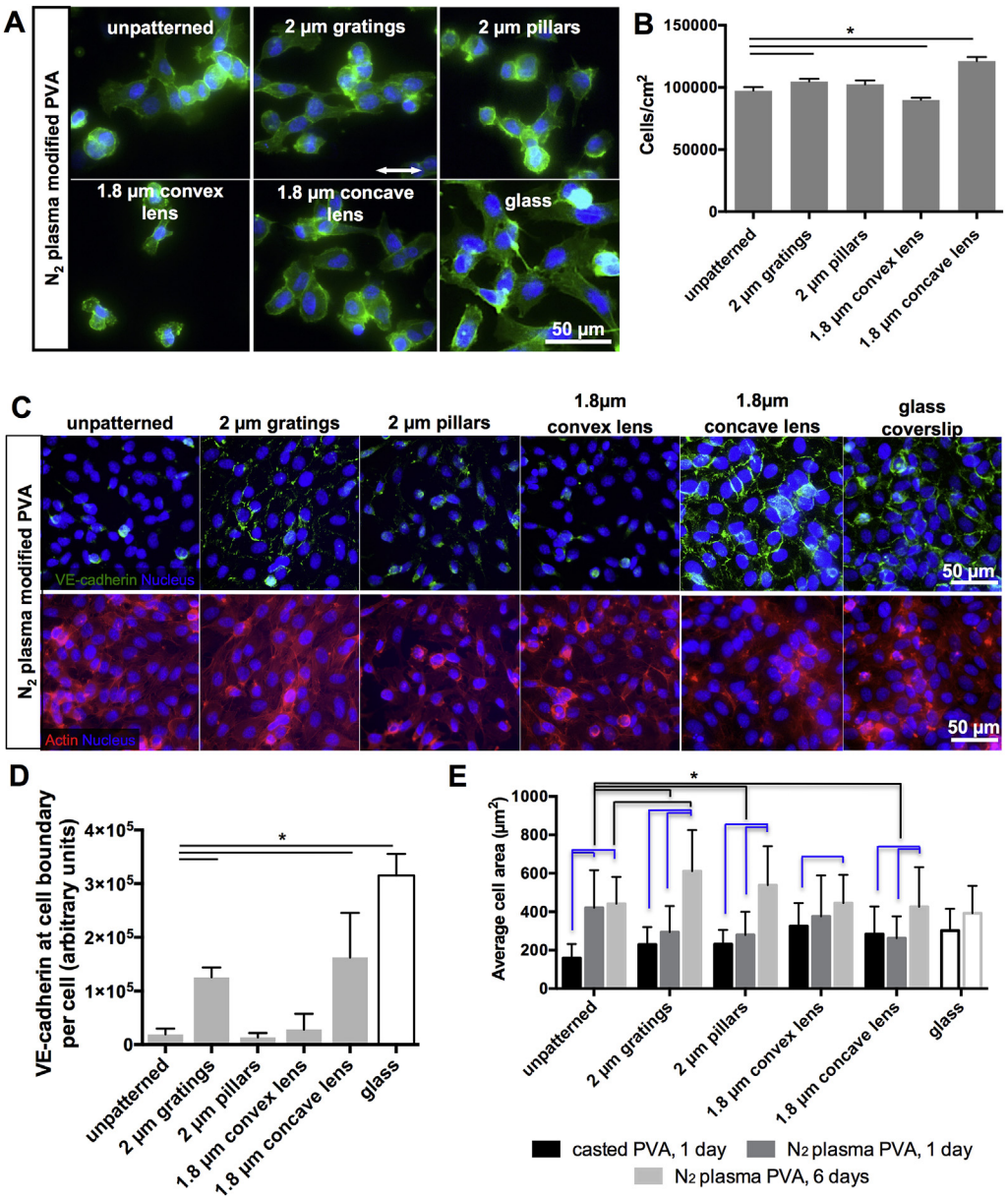

Fig. 6. EC adhesion and area on selected casted PVA with N_2 plasma modification. Unpatterned PVA modified with N_2 plasma were used as controls. (A) Fluorescence images of cells grown on casted PVA films modified with N_2 plasma for 24 h. Blue denotes nuclei, green denotes actin. Scale bar = 50 μm. (B) Average cell density on casted PVA films modified with N_2 plasma after 24 h culture. * denotes statistical significance using one-way ANOVA with $p < 0.01$. Two-way ANOVA indicated that EC density on PVA films modified with N_2 plasma significantly improved from unmodified PVA films with the same topography. (C) EC monolayer function on casted PVA with N_2 plasma modification after 6 days culture. Immunofluorescence staining showed EC monolayer formed on N_2 plasma modified films after 6 days culture. Green denotes vascular endothelial-cadherin (VE-cadherin), red shows actin cytoskeleton and blue denotes nuclei. Scale bar = 50 μm. (D) Quantification of VE-cadherin expression on EC monolayer grown on N_2 modified PVA. *denotes statistical significance using one-way ANOVA with $p < 0.0001$. (E) Analysis of EC area on casted PVA with and without N_2 plasma modification. Values of EC area after 24 h culture on casted PVA films without plasma modification from Fig. 5E were included for comparison. Black and blue lines show statistically significant comparisons of EC area using one-way ANOVA with $p \leq 0.05$. (For interpretation of the references to colour in this figure legend, the reader is referred to the web version of this article.)

expression. Quantitative analysis similarly showed a significant improvement in fluorescence intensity of VE-cadherin detected on EC boundary after culture on N_2 plasma modified PVA with 2 μm gratings or 1.8 concave lens compared to unpatterned (Fig. 6D).

Cell area and circularity were compared between 1 day and 6 day growth period on N_2 plasma treated PVA (Fig. 6E). EC area after 1 day on N_2 plasma modified PVA with 2 μm gratings, 2 μm pillars, and 1.8 μm convex lens significantly decreased as compared to unpatterned PVA with N_2 plasma modification (Fig. 6E, black lines). EC showed a trend of increasing cell area with topography on all N_2 plasma modified PVA, as opposed to cells grown on casted PVA without plasma treatment for 24 h (Fig. 6E, blue lines). A significant enhancement of cell area was also observed when comparing EC cultured for 6 days on N_2 plasma modified PVA with 2 μm gratings. N_2 plasma modified PVA with 2 μm gratings, 2 μm pillars or 1.8 μm concave lens also exhibited a significant difference in EC area when comparing between 24-h and 6-day culture periods. EC area on all N_2 plasma modified PVA, regardless of culture duration or topographical modification, significantly increased from EC area on unpatterned casted PVA.

A similar but opposite, decreasing trend in EC circularity was observed (Figure S4A). However, EC on all PVA substrates still

showed statistically higher circularity compared with those on glass. After 6 days culture, drastic changes were observed between EC on N_2 plasma modified PVA with patterns and without pattern (Figure S4B). EC on N_2 plasma modified PVA with 2 μm gratings exhibited significantly lower cell circularity than EC on N_2 plasma modified PVA without pattern, matching the elongated morphology observed. EC on N_2 plasma modified PVA with 2 μm pillars and 1.8 μm convex lens also showed lower circularity due to the increase in filopodia formation. EC on N_2 plasma modified PVA with 1.8 μm concave lens exhibited higher circularity compared with that on N_2 plasma modified without pattern, which is consistent with the observed cobblestone EC morphology. Significantly, only EC circularity on N_2 plasma modified PVA with 1.8 μm concave lens did not show any significant difference from that on glass control.

3.5. Fabrication of tubular PVA with luminal topography via dip-casting method

Successful patterning of the lumen of PVA tubular scaffolds with both anisotropic and isotropic patterns on its luminal surface was observed (Fig. 7A). Macroscopic evaluation of the lumen showed a uniform surface, with high-fidelity shape replication evident in high magnification. Notably, topographies were observed throughout the length of the PVA tubular scaffold. Furthermore, the mechanical properties of patterned PVA tubular scaffolds such as internal diameter, wall thickness, radial compliance, burst pressure, suture retention and Young's modulus were not significantly altered from unpatterned PVA tubular scaffolds (Table S2). To demonstrate the effect of the luminal topographical modification on improving self-endothelialisation and patency of PVA graft, PVA tubular scaffolds were implanted in a rat abdominal aorta. In the proof-of-concept study, PVA grafts were implanted without anti-coagulant or antiplatelets regime (Fig. 7B). H&E-stained sections showed some nucleate cells in the lumen of PVA grafts with 2 μm gratings, indicative of intimal hyperplasia. Additionally, 2 μm gratings structures on PVA grafts were clearly visible on sections stained with H&E, thus affirming robust patterning that can withstand high shear stress in the aorta. H&E images showed formation of thrombus at the luminal wall of PVA grafts with 2 μm pillars and 1.8 μm concave lens. PVA grafts with 1.8 μm convex lens or without pattern were completely occluded with thrombus at 2 days and 20 days post-implantation, respectively. Meanwhile, partial patency of PVA grafts with 2 μm pillars (3% patent luminal area), 1.8 μm concave lens (24% patent luminal area) and 2 μm gratings (37% patent luminal area) topographies were observed at 20 days (Fig. 7C). Most significantly, EC attachment on the luminal surface of PVA grafts with 2 μm gratings were observed using immunofluorescence (Fig. 7D).

4. Discussion

4.1. Facile and reproducible technique for planar and tubular patterning of PVA

Poly(vinyl alcohol) is widely used for biomedical applications yet there is a need to enhance its biological functionality. Significance of topography on material surfaces in influencing cell behaviour is increasingly exploited in tissue engineering. Yet current techniques for hydrogel patterning are limited to micron-size resolution and require cytotoxic organic solvents.

The ease of modifying PVA hydrogel with faithfully replicated topographies was demonstrated in this study. A challenge in using PDMS stamp for patterning of hydrogel is the lack of wetting due to the hydrophobic surface of PDMS. The introduction of oxygen plasma treated PDMS mold to improve interface wetting and a centrifugation step to remove air bubbles trapped in the topography features were demonstrated to achieve well replicated patterns on PVA via casting.

Both SEM and ESEM revealed that micro-size topography dimensions on casted PVA were consistently smaller from the PDMS mold. Since ESEM operates in a low vacuum and high humidity environment, the size reduction observed cannot be attributed to the dehydration of films during observation. Rather, the loss of water during crosslinking may have caused smaller topography dimensions. As the crosslinking was carried out in a controlled environment, the size reduction was consistently observed for all the patterns. Thus, patterning of PVA via casting method is a well-controlled and repeatable process. For future applications, the reduction in topography dimensions on casted PVA could be accounted for in experimental analysis as the effective dimensions exposed to cells and other biological materials.

However, the combination of the loss of water during the crosslinking process and the incomplete filling resulted in poor replication of nano-size features on casted PVA. Higher resistance of PDMS with nano-size features to capillary force may have hindered complete filling of the PDMS mold [34]. Hence, the added pressure during the imprint system achieved complete filling before crosslinking and greatly improved the fidelity in both shape and size of topographies.

Non-planar patterning is very challenging and limited to non-periodic patterns on non-hydrogel materials. Although previous reports show rolled-up patterned flat films [35,36] and casting on electrospun polyurethane [37], these methods are limited to organic-based polymeric materials. Gadegaard et al. also described a technique that allowed patterning of tubular structures through polymer demixing technique with limitations in uniformity [38].

In order to fabricate topography on non-planar forms, a dip-casting method for simultaneous luminal patterning and macro-molding of a tubular hydrogel achieved high-fidelity and uniform patterning. To the best of our knowledge, this is the first demonstration of a hydrogel-based tubular scaffold with periodic array of topographies less than 10 μm in size to be presented in the lumen. The dip-casting technique was shown to be limited to topographies in the sub-micron range and fabrication of tubular scaffolds with inner diameter of at least 2 mm. In future studies, a uniform cylindrical mold made of materials that have better wetting interaction could permit a wide variety of topographies to be incorporated into the luminal surface for applications in vascular [35] and nerve tissue engineering [36].

4.2. Topographical and N_2 plasma modification of PVA improved EC adhesion and function

Mimicking the biophysical niche on synthetic substrates by using structural cues is a widely used strategy to influence cell behavior *in vitro*. The study supports the notion that mimicking the pits, fibers and bumps [39] found on the EC basement membrane can recapitulate the physiological behaviour and function of EC. Notably, PVA with 2 μm gratings, 1.8 μm convex lens or 1.8 μm concave lens significantly improved EC density, area, morphology, and decreased cell circularity after 1 day. Increase in cell area and decrease in cell circularity are strongly correlated with enhanced cell attachment and cell–substrate interaction via integrin engagement [40], and reduced apoptotic rate [41], respectively. The results in this study aligned with previous reports wherein photo-crosslinked polyethylene glycol hydrogel with gratings with less than 10 μm dimensions enhanced cell-material compared with non-cell adhesive, unpatterned hydrogel [42].

The effect of topography on cell adhesion is widely postulated to

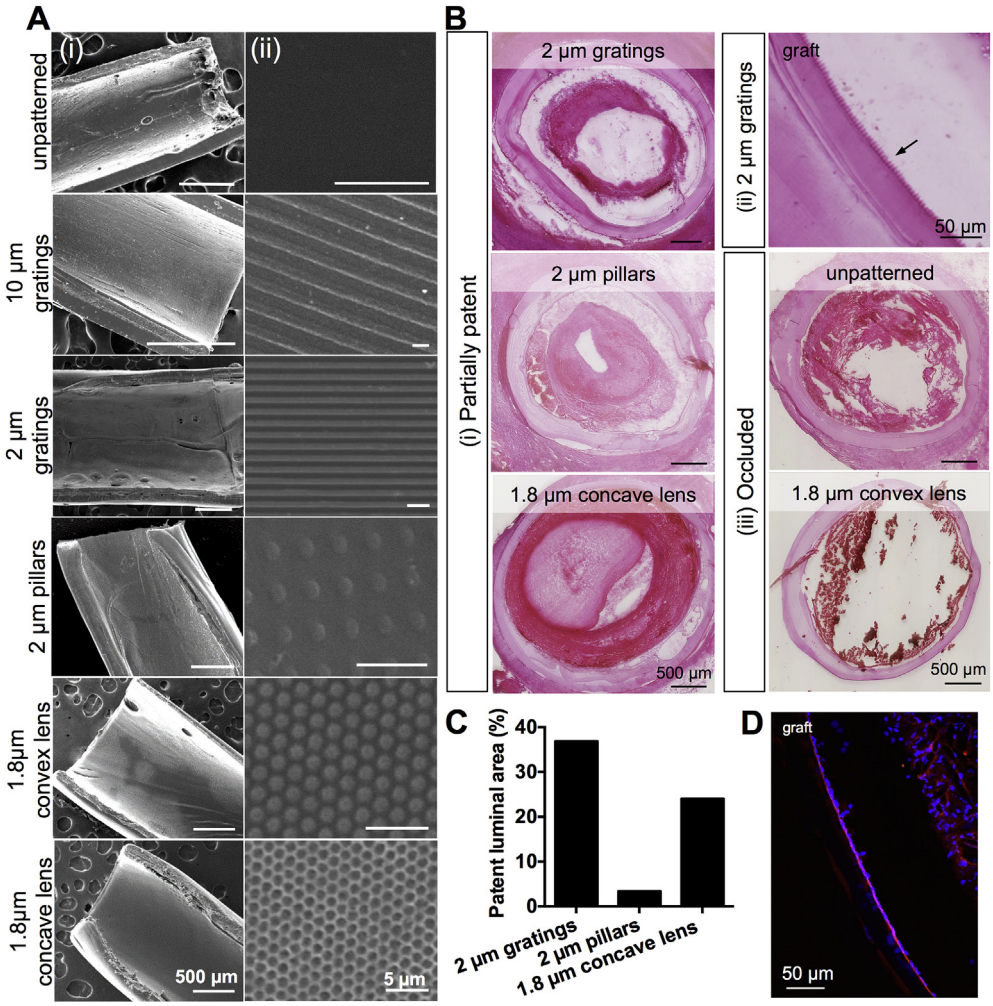

Fig. 7. Fabrication and *in vivo* implantation of tubular PVA grafts with luminal topography. (A) SEM of PVA grafts either unpatterned or patterned with different topographies. (i) The macroscopic view of the tubular patterned PVA grafts. Scale bar = 500 μm. (ii) High magnification of the tubular patterned PVA grafts showed luminal topography. Scale bar = 5 μm. (B) Histological analysis of frozen sections of PVA grafts after explantation from rat abdominal aorta. (i) Standard hematoxylin and eosin (H&E) staining showed partial patency of PVA grafts with 2 μm gratings, 2 μm pillars and 1.8 μm concave lens with apparent luminal tissue narrowing the lumen of the grafts. Scale bar = 500 μm. (ii) Gratings structures on PVA grafts (black arrow) with 2 μm gratings were easily observed through H&E. Scale bar = 50 μm. (iii) H&E shows occlusion of PVA grafts without pattern and with 1.8 μm convex lens. Scale bar = 500 μm. (C) Patent luminal area as a percentage of the total luminal area in partially patent PVA grafts after 20 days. (D) Immunofluorescence staining of explanted PVA graft with 2 μm gratings showed RECA-1 positive endothelial cells (in red) attached to the lumen. Blue denotes nuclei of the cells. Scale bar = 50 μm. (For interpretation of the references to colour in this figure legend, the reader is referred to the web version of this article.)

stem from changes in surface energy and hydrophobicity [43,44]. Our observations with some substrates such as 2 μm gratings PVA provide evidence that hydrophobicity is modified by topography, and that this change in hydrophobicity from the introduction of topography may improve cell adhesion. Indeed, measurement of protein adsorption on the patterned PVA may be performed to further explore the relationship between different types of topography and changes in surface energy and biological response.

N_2 plasma treatment is commonly used for reproducible, controlled and uniform surface modification of biomaterials to enhance material functionality [8,45]. The low-powered N_2 gas plasma treatment employed in this study increased the nitrogen surface content of PVA without distortion of shape or dimension of topographies, similar to what was reported previously [46]. Topography and N_2 plasma modification of PVA resulted in improved EC adhesion, circularity and function. Thus, the synergistic effect of chemical and structural surface modification of PVA aided the formation of a confluent EC monolayer putatively through enhancement of proliferation and inhibition of apoptosis. In addition, the results imply that N_2 plasma modification and concomitant ECM adsorption is more important than topography at an early time point. It may be caused by the necessity for cells to first engage a minimum integrin density to attach and spread [47]. After the initial attachment event (beyond 1 day culture), the effect of topography in cell spreading, proliferation and phenotype was more pronounced.

In fact, the EC monolayer on N_2 plasma modified PVA with 2 μm gratings and 1.8 μm concave lens showed significant improvement in EC function, as shown by VE-cadherin expression. VE-cadherin is critical for preventing endothelial monolayer permeability and decreasing neutrophil transendothelial migration [48]. Despite similar VE-cadherin expression, EC morphology on N_2 plasma modified PVA with these topographies are vastly different. EC morphology on PVA with 1.8 μm concave lens showed high circularity and resembled the cobblestone EC morphology normally observed under static culture *in vitro* [49], on substrates with nano-sized circular protrusions [50] or on fibronectin-rich and atheroprone vessel areas experiencing turbulent flow *in vivo* [51]. Notably,

the EC morphology on PVA with 2 μm gratings showed significantly low circularity and elongation along the gratings axis that resembles the physiological morphology of EC under laminar steady state flow [49], which promotes an anti-thrombogenic [52] and anti-inflammatory phenotype [53]. The 2 μm gratings structures on EC density, area and function may also enhance EC secretion of collagen type IV over fibronectin, which is preferentially secreted by cobblestone EC [54]. Our results consistently demonstrates the beneficial effects of PVA with 2 μm gratings not only for improved EC adhesion, but also for enhanced EC function.

4.3. Tubular patterned PVA grafts as small diameter vascular graft

Many topographies known to direct EC behavior have not yet been applied to vascular grafts due to limitations in tubular patterning. In this study, a surgically implantable and suturable tubular PVA with luminal topography was created. Both *in vitro* and *in vivo* results indicated that the PVA patterned with 2 μm gratings topography would be most beneficial in creating a functioning and intact endothelium in the long-term. In contrast, occlusion was observed in PVA grafts with both 1.8 μm convex and 1.8 μm concave lens. The results may be attributed to increased platelet adhesion on lens topographies *in vitro* [7]. Considering that the animals did not receive any antiplatelet or anticoagulant drugs, it is most plausible that thrombosis of PVA grafts with 1.8 μm convex and 1.8 μm concave lens occurred earlier than endothelial attachment.

5. Conclusion

In summary, we presented casting and NIL as simple and reproducible methods for planar patterning of hydrogel with high yield and patterning integrity. The casting technique presented has high-yield and shape fidelity and can be performed in ambient and aqueous conditions. On the other hand, patterning of nano-sized features with high yield was achieved using NIL. The aid of pressure during the imprint process helped to overcome the capillary force in filling up nano-size structure. PVA with 2 μm gratings, 1.8 μm convex and concave lens significantly improved EC adhesion. Additional plasma treatment of PVA to incorporate amide groups enhanced cell adhesion without altering topographical modification. Notably, PVA with 2 μm gratings and 1.8 μm concave lens topography enhanced EC adhesion and function compared with unpatterned PVA. To aid the integration of topography into useful three-dimensional platforms, a novel non-planar patterning method was developed to achieve luminal micron-size patterns on tubular PVA graft. To our knowledge, this is the first demonstration of hydrogel patterning of a luminal surface with a periodic array of patterns. In a preliminary rat study without anticoagulant and antiplatelet regimen, PVA grafts with 2 μm gratings showed enhanced patency and endothelialisation after 20 days.

Acknowledgments

This research is funded by the Singapore Agency for Science, Technology and Research (A*STAR; 1122703037) and the France National Agency for Research (ANR-10 INTB-1502-01) joint program and the Singapore Ministry of Health's National Medical Research Council, under Exploratory/Developmental Grant Scheme (NMRC/EDG/0068/2009). This work was partially funded by the National Research Foundation Singapore through the Mechanobiology Institute under the Research Centre of Excellence programme. We would like to thank Dr. M. Chaouat for performing the animal surgeries. We also thank Mr Brian Teo for mechanical testing of PVA grafts and Ms Dawn Neo for assistance with water contact angle measurements. We would also like to thank Ms June Ong from A*STAR IMRE SnFPC for help in the preliminary XPS characterization. GSH is supported by the A*STAR Scientific Staff Development Award Program.

Appendix A. Supplementary data

Supplementary data related to this article can be found at http://dx.doi.org/10.1016/j.biomaterials.2016.01.036.

References

[1] S.L. Bourke, M. Al-Khalili, T. Briggs, B.B. Michniak, J. Kohn, L.A. Poole-Warren, A photo-crosslinked poly(vinyl alcohol) hydrogel growth factor release vehicle for wound healing applications, AAPS Pharm. Sci. 5 (2008) 101–111, http://dx.doi.org/10.1208/ps050433.
[2] Y. Jiang, A. Schädlich, E. Amado, C. Weis, E. Odermatt, K. Mäder, et al., In-vivo studies on intraperitoneally administrated poly(vinyl alcohol), J. Biomed. Mater. Res. 93 (2010) 275–284, http://dx.doi.org/10.1002/jbm.b.31585.
[3] F.A. Andersen, Final report on the safety assessment of sodium metaphosphate, sodium trimetaphosphate, and sodium hexametaphosphate, Int. J. Toxicol. 20 (2001) 75–89.
[4] G. Leone, M. Consumi, M. Aggravi, A. Donati, S. Lamponi, A. Magnani, PVA/STMP based hydrogels as potential substitutes of human vitreous, J. Mater. Sci. Mater. Med. 21 (2010) 2491–2500, http://dx.doi.org/10.1007/s10856-010-4092-7.
[5] M. Chaouat, C. Le Visage, W.E. Baille, B. Escoubet, F. Chaubet, M.A. Mateescu, et al., A novel cross-linked poly(vinyl alcohol) (PVA) for vascular grafts, Adv. Funct. Mater. 18 (2008) 2855–2861, http://dx.doi.org/10.1002/adfm.200701261.
[6] M.F.A. Cutiongco, R.K.T. Choo, N.J.X. Shen, B.M.X. Chua, E. Sju, A.W.L. Choo, et al., Composite scaffold of poly(vinyl alcohol) and interfacial polyelectrolyte complexation fibers for controlled biomolecule delivery, Front. Bioeng. Biotechnol. 3 (2015) 3, http://dx.doi.org/10.3389/fbioe.2015.00003.
[7] M.F.A. Cutiongco, D.E.J. Anderson, M.T. Hinds, E.K.F. Yim, In vitro and ex vivo hemocompatibility of off-the-shelf modified poly(vinyl alcohol) vascular grafts, Acta Biomater. 25 (2015) 97–108, http://dx.doi.org/10.1016/j.actbio.2015.07.039.
[8] J.M. Ino, P. Chevallier, D. Letourneur, D. Mantovani, C. Le Visage, Plasma functionalization of poly(vinyl alcohol) hydrogel for cell adhesion enhancement, Biomatter 3 (2013) e25414, http://dx.doi.org/10.4161/biom.25414.
[9] P. Vandrangi, S.C. Gott, R. Kozaka, V.G.J. Rodgers, M.P. Rao, Comparative endothelial cell response on topographically patterned titanium and silicon substrates with micrometer to sub-micrometer feature sizes, PLoS One 9 (2014) e111465, http://dx.doi.org/10.1371/journal.pone.0111465.
[10] S. Ankam, M. Suryana, L.Y. Chan, A.A.K. Moe, B.K.K. Teo, J.B.K. Law, et al., Substrate topography and size determine the fate of human embryonic stem cells to neuronal or glial lineage, Acta Biomater. 9 (2013) 4535–4545, http://dx.doi.org/10.1016/j.actbio.2012.08.018.
[11] R. Muhammad, G.S.L. Peh, K. Adnan, J.B.K. Law, J.S. Mehta, E.K.F. Yim, Micro- and nano-topography to enhance proliferation and sustain functional markers of donor-derived primary human corneal endothelial cells, Acta Biomater. 19 (2015) 138–148, http://dx.doi.org/10.1016/j.actbio.2015.03.016.
[12] B.K.K. Teo, S.-H. Goh, T.S. Kustandi, W.W. Loh, L.H. Yee, E.K.F. Yim, The effect of micro and nanotopography on endocytosis in drug and gene delivery systems, Biomaterials 32 (2011) 9866–9875, http://dx.doi.org/10.1016/j.biomaterials.2011.08.088.
[13] E.K.F. Yim, A.C.A. Wan, C. Le Visage, I.-C. Liao, K.W. Leong, Proliferation and differentiation of human mesenchymal stem cell encapsulated in polyelectrolyte complexation fibrous scaffold, Biomaterials 27 (2006) 6111–6122, http://dx.doi.org/10.1016/j.biomaterials.2006.07.037.
[14] D.S.T. Chong, B. Lindsey, M.J. Dalby, N. Gadegaard, A.M. Seifalian, H. GG, Luminal surface engineering, "micro and nanopatterning": potential for self endothelialising vascular grafts? Eur. J. Vasc. Endovasc. Surg. 47 (2014) 566–576, http://dx.doi.org/10.1016/j.ejvs.2014.02.007.
[15] A. de Mel, C. Bolvin, M. Edirisinghe, G. Hamilton, A.M. Seifalian, Development of cardiovascular bypass grafts: endothelialization and applications of nanotechnology, Expert Rev. Cardiovasc Ther. 6 (2008) 1259–1277, http://dx.doi.org/10.1586/14779072.6.9.1259.
[16] P. Pavli, P.S. Petrou, A.M. Douvas, Protein-resistant crosslinked poly (vinyl alcohol) micropatterns via photolithography using removable polyoxometalate photocatalyst, ACS Appl. Mater. Interfaces 6 (20) (2014) 17463–17473.
[17] M.L. Pourciel, J. Launay, W. Sant, V. Conédéra, A. Martinez, P. Temple-Boyer, Development of photo-polymerisable polyvinyl alcohol for biotechnological applications, Sens. Actuators B Chem. 94 (2003) 330–336, http://dx.doi.org/10.1016/S0925-4005(03)00463-5.
[18] S. Rodriguez Vilches, C. Séverac, C. Thibaut, L. Laplatine, C. Vieu, J. Fitremann, et al., Nanostructuration of soft hydrogels: synthesis and characterization of saccharidic methacrylate gels, Colloid Polym. Sci. 289 (2011) 1437–1449, http://dx.doi.org/10.1007/s00396-011-2465-1.
[19] G. Papavasiliou, P. Songprawat, V. Pérez-Luna, E. Hammes, M. Morris, Y.-

C. Chiu, et al., Three-dimensional patterning of poly (ethylene glycol) hydrogels through surface-initiated photopolymerization, Tissue Eng. Part C. Methods 14 (2008) 129–140.
[20] A.B. Faia-Torres, T. Goren, M. Textor, M. Pla-Roca, Patterned Biointerfaces, Elsevier Ltd, 2011, http://dx.doi.org/10.1016/B978-0-08-055294-1.00260-9.
[21] M. Nikkhah, N. Eshak, P. Zorlutuna, N. Annabi, M. Castello, K. Kim, et al., Directed endothelial cell morphogenesis in micropatterned gelatin methacrylate hydrogels, Biomaterials (2012) 1–10, http://dx.doi.org/10.1016/j.biomaterials.2012.08.068.
[22] R.S. Kane, S. Takayama, E. Ostuni, D.E. Ingber, G.M. Whitesides, Patterning proteins and cells using soft lithography, Biomaterials 20 (1999) 2363–2376.
[23] Y. Xia, G.M. Whitesides, Soft lithography, Annu. Rev. Mater. Sci. 28 (1998) 153–184.
[24] F. Di Benedetto, A. Biasco, D. Pisignano, R. Cingolani, Patterning polyacrylamide hydrogels by soft lithography, Nanotechnology 16 (2005) S165.
[25] S. Kobel, M. Limacher, S. Gobaa, T. Laroche, M.P. Lutolf, Micropatterning of hydrogels by soft embossing †, Langmuir 25 (2009) 8774–8779, http://dx.doi.org/10.1021/la9002115.
[26] C.-M. Cheng, P.R. LeDuc, Micropatterning polyvinyl alcohol as a biomimetic material through soft lithography with cell culture, Mol. Biosyst. 2 (2006) 299–303, http://dx.doi.org/10.1039/b606496p.
[27] S.Y. Chou, P.R. Krauss, W. Zhang, L. Guo, L. Zhuang, Sub-10 nm imprint lithography and applications, J. Vac. Sci. Technol. B 15 (1997) 2897–2904, http://dx.doi.org/10.1116/1.589752.
[28] C.D. Schaper, Planarizing surface topography by polymer adhesion to water-soluble templates with replicated null pattern, Langmuir 20 (2004) 227–231.
[29] A.M.H. Ng, Y. Wang, W.C. Lee, C.T. Lim, K.P. Loh, L.H. Yee, Patterning of graphene with tunable size and shape for microelectrode array devices, Carbon 67 (2014) 390–397, http://dx.doi.org/10.1016/j.carbon.2013.10.009.
[30] M.S. Peresin, A.H. Vesterinen, Y. Habibi, Crosslinked PVA nanofibers reinforced with cellulose nanocrystals: water interactions and thermomechanical properties, J. Appl. Polym. Sci. 131 (11) (2014), http://dx.doi.org/10.1002/app.40334.
[31] A. Mousa, G. Heinrich, F. Simon, U. Wagenknecht, Carboxylated nitrile butadiene rubber/hybrid filler composites, Materials 15 (2012) 671–678, http://dx.doi.org/10.1590/S1516-14392012005000086.
[32] R.J. McMurray, N. Gadegaard, P.M. Tsimbouri, K.V. Burgess, L.E. McNamara, R. Tare, et al., Nanoscale surfaces for the long-term maintenance of mesenchymal stem cell phenotype and multipotency, Nat. Mater. 10 (2011) 637–644, http://dx.doi.org/10.1038/nmat3058.
[33] M.F.A. Cutiongco, R.K.T. Choo, N.J.X. Shen, B.M.X. Chua, E. Sju, A.W.L. Choo, et al., Composite scaffold of poly(vinyl alcohol) and interfacial polyelectrolyte complexation fibers for controlled biomolecule delivery, Front. Bioeng. Biotechnol. 3 (2015) 3, http://dx.doi.org/10.3389/fbioe.2015.00003.
[34] K.Y. Suh, H.H. Lee, Capillary force lithography: large-area patterning, self-organization, and anisotropic dewetting, Adv. Funct. Mater. 12 (2002) 405–413.
[35] P. Zorlutuna, N. Hasirci, V. Hasirci, Nanopatterned collagen tubes for vascular tissue engineering, J. Tissue Eng. Regen. Med. 2 (2008) 373–377, http://dx.doi.org/10.1002/term.99.
[36] H.C. Ni, Z.Y. Lin, S.H. Hsu, I.M. Chiu, The use of air plasma in surface modification of peripheral nerve conduits, Acta Biomater. 6 (2010) 2066–2076, http://dx.doi.org/10.1016/j.actbio.2009.12.038.
[37] P. Uttayarat, A. Perets, M. Li, P. Pimton, S.J. Stachelek, I. Alferiev, et al., Micropatterning of three-dimensional electrospun polyurethane vascular grafts, Acta Biomater. 6 (2010) 4229–4237, http://dx.doi.org/10.1016/j.actbio.2010.06.008.
[38] N. Gadegaard, M.J. Dalby, M.O. Riehle, A.S.G. Curtis, S. Affrossman, Tubes with controllable internal nanotopography, Adv. Mater. 16 (2004) 1857–1860, http://dx.doi.org/10.1002/adma.200400408.
[39] S.J. Liliensiek, P. Nealey, C.J. Murphy, Characterization of endothelial basement membrane nanotopography in rhesus macaque as a guide for vessel tissue engineering, Tissue Eng. Part A 15 (2009) 2643–2651, http://dx.doi.org/10.1089/ten.TEA.2008.0284.
[40] S.P. Massia, J.A. Hubbell, An RGD spacing of 440 nm is sufficient for integrin alpha V beta 3-mediated fibroblast spreading and 140 nm for focal contact and stress fiber formation, J. Cell Biol. 114 (1991) 1089–1100.
[41] C.S. Chen, M. Mrksich, S. Huang, G.M. Whitesides, D.E. Ingber, Geometric control of cell life and death, Science 276 (1997) 1425–1428.
[42] V.A. Schulte, M. Diez, M. Möller, M.C. Lensen, Surface topography induces fibroblast adhesion on intrinsically nonadhesive poly(ethylene glycol) substrates, Biomacromolecules 10 (2009) 2795–2801, http://dx.doi.org/10.1021/bm900631s.
[43] J. Carpenter, D. Khang, T.J. Webster, Nanometer polymer surface features: the influence on surface energy, protein adsorption and endothelial cell adhesion, Nanotechnology 19 (2008) 505103, http://dx.doi.org/10.1088/0957-4484/19/50/505103.
[44] M.B. Hovgaard, K. Rechendorff, J. Chevallier, M. Foss, F. Besenbacher, Fibronectin adsorption on tantalum: the influence of nanoroughness, J. Phys. Chem. B 112 (2008) 8241–8249, http://dx.doi.org/10.1021/jp801103n.
[45] M.R. Sanchis, O. Calvo, O. Fenollar, D. Garcia, R. Balart, Characterization of the surface changes and the aging effects of low-pressure nitrogen plasma treatment in a polyurethane film, Polym. Test. 27 (2008) 75–83, http://dx.doi.org/10.1016/j.polymertesting.2007.09.002.
[46] D. Sankar, K.T. Shalumon, K.P. Chennazhi, D. Menon, R. Jayakumar, Surface plasma treatment of poly(caprolactone) micro, nano, and multiscale fibrous scaffolds for enhanced osteoconductivity, Tissue Eng. Part A 20 (2014) 1689–1702, http://dx.doi.org/10.1089/ten.tea.2013.0569.
[47] G. Le Saux, A. Magenau, T. Böcking, K. Gaus, J.J. Gooding, The relative importance of topography and RGD ligand density for endothelial cell adhesion, PLoS One 6 (2011) e21869, http://dx.doi.org/10.1371/journal.pone.0021869.s005.
[48] P.L. Hordijk, E. Anthony, F.P. Mul, R. Rientsma, L.C. Oomen, D. Roos, Vascular-endothelial-cadherin modulates endothelial monolayer permeability, J. Cell Sci. 112 (12) (1999) 1915–1923.
[49] S. Noria, D.B. Cowan, A.I. Gotlieb, B.L. Langille, Transient and steady-state effects of shear stress on endothelial cell adherens junctions, Circ. Res. 85 (1999) 504–514.
[50] M. Schernthaner, B. Reisinger, H. Wolinski, S.D. Kohlwein, A. Trantina-Yates, M. Fahrner, et al., Nanopatterned polymer substrates promote endothelial proliferation by initiation of β-catenin transcriptional signaling, Acta Biomater. 8 (2012) 2953–2962, http://dx.doi.org/10.1016/j.actbio.2012.04.018.
[51] R.M. Nerem, Hemodynamics and the vascular endothelium, J. Biomech. Eng. 115 (1993) 510–514.
[52] C. Di Rienzo, E. Jacchetti, F. Cardarelli, R. Bizzarri, F. Beltram, M. Cecchini, Unveiling LOX-1 receptor interplay with nanotopography: mechanotransduction and atherosclerosis onset, Sci. Rep. 3 (2013) 1–8, http://dx.doi.org/10.1038/srep01141.
[53] K.B. Vartanian, M.A. Berny, O.J.T. McCarty, S.R. Hanson, M.T. Hinds, Cytoskeletal structure regulates endothelial cell immunogenicity independent of fluid shear stress, AJP Cell Physiol. 298 (2010) C333–C341, http://dx.doi.org/10.1152/ajpcell.00340.2009.
[54] K.B. Vartanian, S.J. Kirkpatrick, O.J.T. McCarty, T.Q. Vu, S.R. Hanson, M.T. Hinds, Distinct extracellular matrix microenvironments of progenitor and carotid endothelial cells, J. Biomed. Mater. Res. A 91 (2009) 528–539, http://dx.doi.org/10.1002/jbm.a.32225.